THEORETICAL & APPLIED MECHANICS LETTERS **2**, 021001 (2011)

Controlled buckling of thin film on elastomeric substrate in large deformation

C. Chen,[1] W. Tao,[2] Z. J. Liu,[3] Y. W. Zhang,[3] and J. Song[1, a)]

[1)] *Department of Mechanical and Aerospace Engineering, University of Miami, Coral Gables, FL 33146*
[2)] *Institute of Applied Mechanics, Zhejiang University, Hangzhou 310027, China*
[3)] *Institute of High Performance Computing, 1 Fusionopolic Way, #16-16 Connexis, 138632, Singapore*

(Received 05 February 2011; accepted 12 February 2011; published online 10 March 2011)

Abstract Electronic systems with large stretchability have many applications. A precisely controlled buckling strategy to increase the stretchability has been demonstrated by combining lithographically patterned surface bonding chemistry and a buckling process. The buckled geometry was assumed to have a sinusoidal form, which may result in errors to determine the strains in the film. A theoretical model is presented in this letter to study the mechanics of this type of thin film/substrate system by discarding the assumption of sinusoidal buckling geometry. It is shown that the previous model overestimates the deflection and curvature in the thin film. The results from the model agree well with finite element simulations and therefore provide design guidelines in many applications ranging from stretchable electronics to micro/nano scale surface patterning and precision metrology. © *2011 The Chinese Society of Theoretical and Applied Mechanics.* [doi:10.1063/2.1102101]

Keywords thin film, buckling, large deformation

Stretchable electronics enables many new applications such as flexible displays,[1] electronic eye camera,[1–4] conformable skin sensors,[5] smart surgical gloves,[6] and structural health monitoring devices.[7] Circuits that use organic semiconductor materials can sustain large deformations,[8–10] but their electronical performance is relatively poor comparing to conventional inorganic materials such as silicon. It is critical to use the high performance conventional inorganic material (e.g., silicon) to develop stretchable electronics. Since all known inorganic semiconductor materials are brittle and fracture at strains of the order of 1 percent, sophisticated designs are required to make these inorganic materials stretchable. One of the most intuitive approaches is to produce stretchable components directly based on periodic wavy shaped ribbons (or membranes) bonded at all points on elastomeric substrates.[11–13] The wavelengths and amplitudes, which are determined by material properties (e.g., moduli and thickness) without any direct control, of the waves can change to accommodate strains ($\sim$ 20%) in a way that involves small strains in the ribbons.[14–16] In a related approach, the ribbons can be designed to bond to the elastomeric substrate only at certain locations,[17] which has the advantage that the wavelengths can be defined precisely with a level of engineering control to have a higher stretchability. Figure 1 schematically illustrates the fabrication process,[17] which combines lithographically patterned surface bonding chemistry and a buckling process. Figure 1(a) shows the bonding chemistry on a pre-stretched poly(dimethylsiloxane) (PDMS) substrate with prestrain $\varepsilon_{pre} = \Delta L/L$ along the ribbon direction. Let L_0' denote the width of activated regions, where chemical bonding occurs between the ribbons (e.g., Si) and the PDMS substrate and L_0 the width of inactivated regions, where only weak van der Waals interactions occur at the interface. Thin ribbons are then attached to the prestrained and patterned PDMS substrate (Fig. 1(b)) with the ribbon direction parallel to the prestreched direction. Releasing the prestrain leads to compression, which causes the ribbons on the inactivated regions to buckle and move out of the plane of the substrate (Fig. 1c). The wavelength of the buckled structures is then given by $L_1 = L_0/(1+\varepsilon_{pre})$ due to the geometrical constrain as shown in Fig. 2.

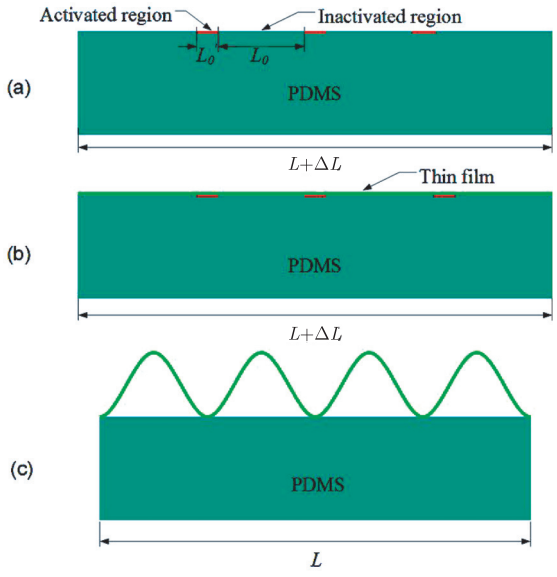

Fig. 1. Schematically illustration of the fabrication process for controlled buckled thin film.

Jiang et al.[18] developed an analytical model without considering the finite geometry change (i.e., the differ-

a)Corresponding author. Email: jsong8@miami.edu.

ence between the undeformed and deformed configuration) to study the buckling behavior of such systems. The buckling profile of the ribbon is assumed to be a sinusoidal form $w = \frac{1}{2}A\left(1-\cos 2\pi x/L_1\right)$, which satisfies vanishing displacement and slope at the two ends $x = 0$ and $x = L_1$. The amplitude A is determined by the energy method. The above model is referred as *small deformation model* in this paper. For small prestrain (<10%), the buckle profile can be represented by the above sinusoidal form and their models agree well with experiments. As the prestrain increases, the buckle profile will not have a sinusoidal form and there will be a discrepancy between the existing model and experiments.[17–19] In addition, the rotation at the two ends will also not be zero since the substrate is compliant.

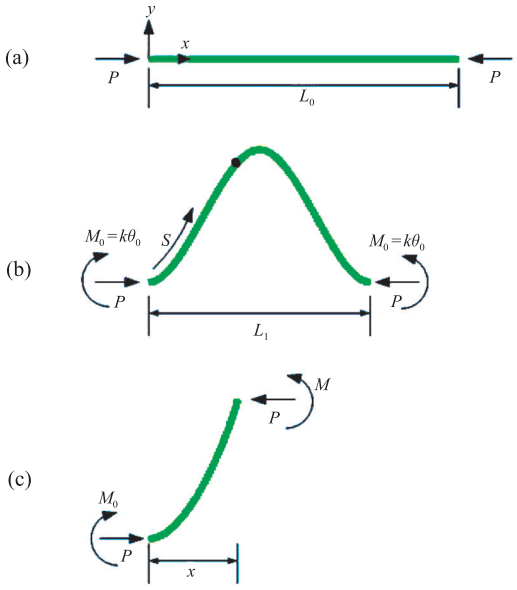

Fig. 2. Schematic diagram of mechanics model for the thin film with torsional springs at the two ends.

This paper aims to establish a mechanics model to describe the deformation of the buckled thin film by discarding the assumption of the sinusoidal form for buckled profile. The non-vanishing rotation at the ends due to the substrate is accounted by a rotational spring with a constant spring constant.

The thin film is modeled as an elastic beam because its thickness (~0.1 μm) is much smaller than any characteristic length such as the wavelength (~100 μm) and film width and length. Consider the initial, strain-free configuration of the beam (Fig. 2a) with bending rigidity EI and length L_0, the ends are attached to elastic rotational springs with the spring constant k. For a beam with the Young's modulus E and uniform thickness h, the bending rigidity $EI = \bar{E}h^3/12$, where $\bar{E} = E/\left(1-\nu^2\right)$ is the plane-strain modulus, and ν is the Poisson's ratio. Figure 2(b) shows the deformed configuration and forces acting on the beam. The bending moment M_0 and the rotation θ_0 through the torsional spring constant at the ends are related by $M_0 = k\theta_0$. The limit $k \to \infty$ corresponds to a doubly-clamped beam and the other limit $k \to 0$ corresponds to a simply-supported beam. The left end is fixed and right end has a displacement $u = L_0 - L_1$ to the left, where L_1 is the deformed span length. Instead of using the coordinate (x, y), it is more convenient to work with the intrinsic coordinate (s,θ), where s is the arc length from the left end to a point on the deformed shape and θ is the slope angle at that point. The coordinate (x, y) is related to (s,θ) by $\mathrm{d}x/\mathrm{d}s = \cos\theta$ and $\mathrm{d}y/\mathrm{d}s = \sin\theta$. The equilibrium equation of the beam as shown in Fig. 2(c) is then given by

$$EI\frac{\mathrm{d}\theta}{\mathrm{d}s} = k\theta_0 - Py, \tag{1}$$

where P is the compressive load at the ends. The boundary conditions are

$$\begin{aligned} &x(0) = 0, x(L_0) = L_0 - u, \\ &y(0) = 0, y(L_0) = 0, \\ &\theta(0) = \theta_0, \theta(L_0) = \pi - \theta_0. \end{aligned} \tag{2}$$

By introducing the following non-dimensional terms $\bar{x} = x/L_0$, $\bar{y} = y/L_0$, $\bar{s} = s/L_0$, $\bar{k} = kL_0/EI$, $\bar{P} = PL_0^2/EI$ and $\bar{u} = u/L_0$, Equations (1) and (2) can be written in non-dimensional form as

$$\frac{\mathrm{d}\theta}{\mathrm{d}\bar{s}} + \bar{P}y = \bar{k}\theta_0, \tag{3}$$

and

$$\begin{aligned} &\bar{x}(0) = 0, \bar{x}(1) = 1 - \bar{u}, \\ &\bar{y}(0) = 0, \bar{y}(1) = 0, \\ &\theta(0) = \theta_0, \theta(1) = \pi - \theta_0. \end{aligned} \tag{4}$$

Equations (3) and (4) give

$$\frac{\mathrm{d}\theta}{\mathrm{d}\bar{s}} = \pm\sqrt{4\bar{P}C^2 - 4\bar{P}\sin^2\frac{\theta}{2}}, \tag{5}$$

where C satisfies

$$4\bar{P}C^2 = \left(\bar{k}\theta_0\right)^2 + 4\bar{P}\sin^2\frac{\theta_0}{2}. \tag{6}$$

The plus and minus sign distinguish between buckling to the top and to the bottom. In the following, only the minus sign is considered. Equation (5) then becomes

$$\frac{\mathrm{d}\varphi}{\sqrt{1 - C^2\sin^2\varphi}} = -\sqrt{\bar{P}}\mathrm{d}\bar{s}, \tag{7}$$

where $\sin(\theta/2) = C\sin\varphi$. Integrating Eq. (7) from the end $(\bar{s} = 0, \varphi = \varphi_1)$ of the beam to the mid-length $\left(\bar{s} = \frac{1}{2}, \varphi = 0\right)$ gives

$$\int_0^{\varphi_1} \frac{\mathrm{d}\varphi}{\sqrt{1 - C^2\sin^2\varphi}} = \frac{1}{2}\sqrt{\bar{P}}, \tag{8}$$

where φ_1 satisfies

$$\sin(\theta_0/2) = C\sin\varphi_1. \tag{9}$$

For any given θ_0, C, $\bar{P}$, and φ_1 can be solved by Eqs. (6), (8) and (9). The shortening $\bar{u}$ (i.e., compressive strain $\varepsilon = (L_0 - L_1)/L_0 = \varepsilon_{pre}/(1+\varepsilon_{pre})$) and maximum deflection $\bar{y}_{\max}$ of the beam are then obtained as $\varepsilon = \bar{u} = 2 - 4\int_0^{\varphi_1}\sqrt{1 - C^2\sin^2\varphi}\,\mathrm{d}\varphi/\sqrt{\bar{P}}$, and $\bar{y}_{\max} = 2C(1-\cos\varphi_1)/\sqrt{\bar{P}}$.

The finite element method is also used to study the buckling of thin film in order to validate the above analytical solution. The thin film is modeled by the beam element (B21 in the ABAQUS) and the substrate by the 4-node plane-strain element (CPE4). The thin film and substrate share the same nodes at the interface of the active regions. We first determine the eigenvalues and eigenmodes of the film/substrate system. The first eigenmode is then used as initial small geometrical imperfection to trigger the buckling of the system. The imperfections are always small enough to ensure that the solution is correct.

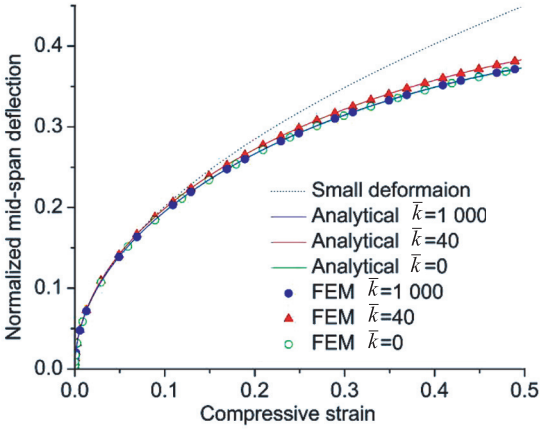

Fig. 3. The normalized mid-span deflection $\bar{y}_{\max}$ versus the compressive strain ε with different normalized torsional spring constant $\bar{k}$.

Figure 3 shows normalized mid-span deflection $\bar{y}_{\max}$ versus the compressive strain ε with different normalized torsional spring constant $\bar{k}$. The results from the current model are shown in solid line, which agree well with the finite element simulations in dot. It should be noted that $\bar{y}_{\max}$ is almost the same for double-clamped ($\bar{k}$= 1000) and simple-supported ends ($\bar{k}$= 0), while $\bar{y}_{\max}$ becomes slightly larger for mid-value $\bar{k}$. For example, $\bar{y}_{\max}$ for $\bar{k}$ = 40 is 3% larger than that for $\bar{k}$= 0 at ε=50%. The previous small deformation model (dotted line)[14] is also shown in Fig. 3 and it clearly shows that the small deformation model will overestimate the deflection about 20% at ε=50%.

The strain in the buckled thin film is dominated by the bending strain,[14–16,20,21] which results from the thin film curvature and is important to determine the

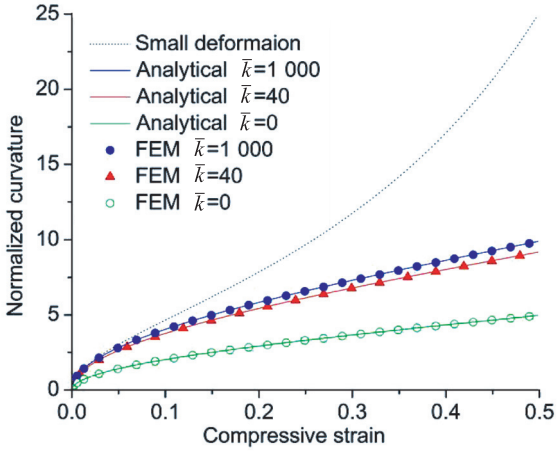

Fig. 4. The normalized maximum curvature $\bar{\kappa} = L_0\kappa_{\max}$ versus the compressive strain ε with different normalized torsional spring constant $\bar{k}$.

stretchability/compressibility of the thin film. Figure 4 shows the normalized maximum curvature $\bar{\kappa} = L_0\kappa_{\max}$ versus the compressive strain ε with different normalized torsional spring constant $\bar{k}$. This figure is very helpful to determine the strains in the thin film. As the compressive strain increases, the curvature increases for both the current (solid line) and previous small deformation (dotted line) models. However, the curvature of small deformation model increases much faster than that of current model. For example, at 50% compressive strain, small deformation model curvature is 3.0 times higher than that of current model with a $\bar{k}$=1000. Figure 4 also shows that as the normalized torsional spring constant $\bar{k}$ increases, the curvature increases. The simple-supported beam ($\bar{k}$=0) has the lowest normalized curvature 4.97 at 50% compressive strain while the double-clamped beam has the largest normalized curvature 10.0 at the same strain level. The finite element simulations have been used to validate the analytical results as shown in Figure 4.

The torsional spring constant in the current model depends on the substrate as well as the dimensions of the thin film (i.e., thickness and width of activated/inactivated regions). The PDMS/Si thin film system is studied here using finite element software ABAQUS. Figure 5 shows the film thickness effect on the normalized torsional spring constant $\bar{k}$. The widths of activated and inactivated region are 10 μm and 200 μm, respectively. It shows that $\bar{k}$ drops drastically when the thin film thickness increases from 0 to 0.5 μm, and then remains a constant $\sim$ 40 as the thickness further increases. The effect of width of activated/inactivated region on the normalized torsional spring constant $\bar{k}$ is shown in Fig. 6. The thin film thickness is 0.1 μm. With increasing the width of inactive region from 100 μm, the normalized $\bar{k}$ increases almost linearly from 40. Increasing the width of activated region also increases

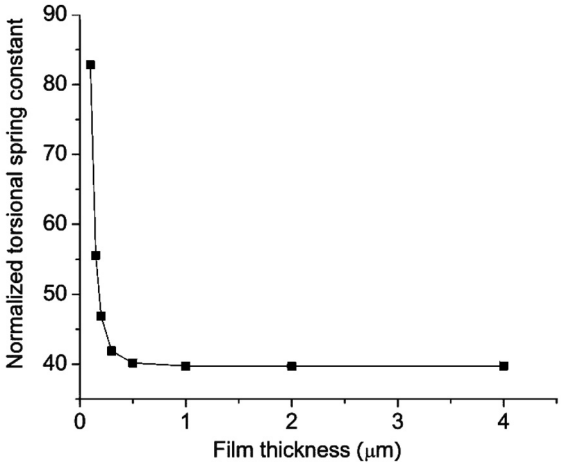

Fig. 5. The thin film thickness effect on the normalized torsional spring constant $\bar{k}$.

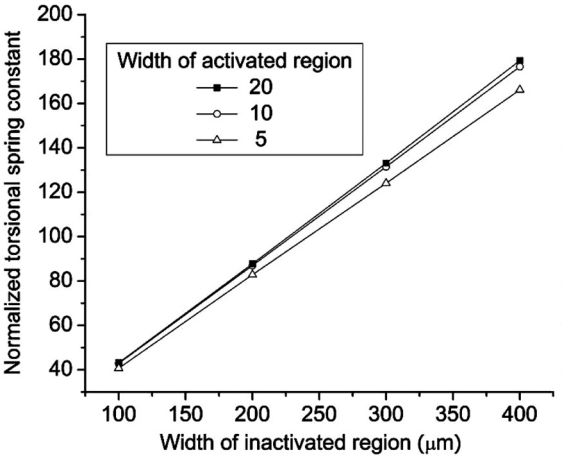

Fig. 6. The effect of width of activated/inactivated region on the normalized torsional spring constant $\bar{k}$.

the normalized $\bar{k}$ but the effect is negligible. Figures 5 and 6 give some guidelines to determine the normalized $\bar{k}$ in the current model. For example, for typical dimensions (width of activated region $>$ 5μm, width of inactivated region $>$ 100μm, and film thickness $>$ 0.1 μm), $\bar{k}$ is larger than 40. Figures 3 and 4 show that the ends can be assumed to be double clamped ($\bar{k}$=1000) since the difference on deflection and curvature are within 5% comparing with $\bar{k}$=40.

In conclusion, a mechanics model is developed to study the deformation of buckled thin film by discarding the assumption of the sinusoidal form for buckled profile and it agrees well with finite element simulations.

This work was supported by the Provost Award (University of Miami), the Ralph E. Powe Junior Faculty Enhancement Award (ORAU), NSF (Grant No. OISE1043161), and NSFC (Grant No.10972194).

1. G.P. Crawford, *Flexible flat panel display technology* (John Wiley & Sons, Ltd., New York, 2005).
2. H.C.Jin, J.R. Abelson, M.K. Erhardt and R.G. Nuzzo, J. Vac. Sci. Technol. B. **22**, 2548 (2004).
3. H.C.Ko, M.P. Stoykovich, J. Song, V. Malyarchuk, W.M. Choi, C.J. Yu, J.B. Geddes, J. Xiao, S. Wang, Y. Huang, and J.A. Rogers, Nature. **454**, 748 (2008).
4. G. Shin, I. Jung, V. Malyarchuk, J. Song, S. Wang, H.C. Ko, Y. Huang, J.S. Ha, and J.A. Rogers, Small. **6**, 851 (2010).
5. V.J. Lumelsky, M.S. Shur, S. Wagner, IEEE Sens. J. **1**, 41 (2001).
6. T. Someya, T. Sekitani, S. Iba, Y. Kato, H. Kawaguchi, and T. Sakurai, P. Natl. Acad. Sci. Usa. **101**, 9966 (2004).
7. A. Nathan, B. Park, A. Sazonov, S. Tao, I. Chan, P. Servati, K. Karim, T. Charania, D. Ma, Q. Striakhilev, and R.V.R. Murthy, Microelectron. J. **31**, 883 (2000).
8. B. Crone, A. Dodabalapur, Y.Y. Lin, R.W. Filas, Z. Bao, A. LaDuca, R. Sarpeshkar, H.E. Katz, and W. Li, Nature. **403**, 521 (2000).
9. Y. L. Loo, T. Someya, K. W. Baldwin, Z. Bao, P. Ho, A. Dodabalapur, H. Katz, and J. A. Rogers, Proc. Natl. Acad. Sci. **99**, 10252 (2002).
10. T. Sekitani, Y. Noguchi, K. Hata, T. Fukushima, T. Aida, and T. Someya, Science **321**, 1468 (2008).
11. N. Bowden, S. Brittain, A. G. Evans, J. W. Hutchinson, and G. M. Whitesides, G.M., Nature **393**, 146 (1998).
12. D. Y. Khang, H. Jiang, Y. Huang, and J. A. Rogers, Science **311**, 208 (2006).
13. W. M. Choi, J. Song, D. Y. Khang, H. Jiang, Y. Huang, and J. A. Rogers, Nano Lett. **7**, 1655 (2007).
14. H. Jiang, D. Y. Khang, J. Song, Y. Sun, Y. Huang, and J. A. Rogers, Proc. Natl. Acad. Sci. **104**, 15607 (2007).
15. J. Song, H. Jiang, Z. Liu, D. Y. Khang, Y. Huang, J. A. Rogers, C. Lu, and C. G. Koh, Int. J. Solids Struct. **45,** 3107 (2008).
16. J. Song, H. Jiang, W. M. Choi, D. Y. Khang, Y. Huang, and J. A. Rogers, J. Appl. Phys. **103**, 014303 (2008).
17. Y. Sun, W. M. Choi, H. Jiang, Y. Huang, J. A. Rogers, Nat. Nanotechnol. **1**, 201 (2006).
18. H. Jiang, Y. Sun, J. A. Rogers, and Y. Huang, Appl. Phys. Lett. **90**, 133119 (2007).
19. H. Jin, W. Y. Lu, M. J. Cordill, and K. Schmidegg, Exp. Mech. **51**, 219 (2010).
20. J. Song, Y. Huang, J. Xiao, S. Wang, K. C. Hwang, H. C. Ko, D. H. Kim, M. P. Stoykovich, and J. A. Rogers, J. Appl. Phys. **105**, 123516. (2009)
21. J. Song, H. Jiang, Y. Huang, and J. A. Rogers, J. Vac. Sci. Technol. A **27,** 1107 (2009).